

Three on Three: Universal and High-Affinity Molecular Recognition of the Symmetric Homotrimeric Spike Protein of SARS-CoV-2 with a Symmetric Homotrimeric Aptamer

Jiuxing Li, Zijie Zhang, Jimmy Gu, Ryan Amini, Alexandria G. Mansfield, Jianrun Xia, Dawn White, Hannah D. Stacey, Jann C. Ang, Gurpreet Panesar, Alfredo Capretta, Carlos D. M. Filipe, Karen Mossman, Bruno J. Salena, Jonathan B. Gubbay, Cynthia Balion, Leyla Soleymani, Matthew S. Miller, Deborah Yamamura, John D. Brennan,* and Yingfu Li*



Cite This: *J. Am. Chem. Soc.* 2022, 144, 23465–23473



Read Online

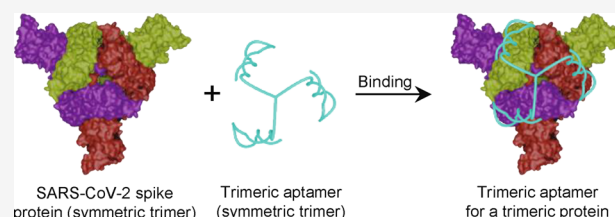
ACCESS |

Metrics & More

Article Recommendations

Supporting Information

ABSTRACT: Our previously discovered monomeric aptamer for SARS-CoV-2 (MSA52) possesses a universal affinity for COVID-19 spike protein variants but is ultimately limited by its ability to bind only one subunit of the spike protein. The symmetrical shape of the homotrimeric SARS-CoV-2 spike protein presents the opportunity to create a matching homotrimeric molecular recognition element that is perfectly complementary to its structural scaffold, causing enhanced binding affinity. Here, we describe a branched homotrimeric aptamer with three-fold rotational symmetry, named TMSA52, that not only possesses excellent binding affinity but is also capable of binding several SARS-CoV-2 spike protein variants with picomolar affinity, as well as pseudotyped lentiviruses expressing SARS-CoV-2 spike protein variants with femtomolar affinity. Using Pd–Ir nanocubes as nanozymes in an enzyme-linked aptamer binding assay (ELABA), TMSA52 was capable of sensitively detecting diverse pseudotyped lentiviruses in pooled human saliva with a limit of detection as low as 6.3×10^3 copies/mL. The ELABA was also used to test 50 SARS-CoV-2-positive and 60 SARS-CoV-2-negative patient saliva samples, providing sensitivity and specificity values of 84.0 and 98.3%, respectively, thus highlighting the potential of TMSA52 for the development of future rapid tests.



INTRODUCTION

The adaptation of symmetric, multimeric proteins to selectively bind DNA sequences is a naturally occurring phenomenon in biological systems.¹ Their interdependent, molecular scaffolds create one cohesive binding site for the recognition of a DNA substrate. Type II restriction enzymes, such as *EcoRV*, are just one of many examples of dimeric proteins that rely on two identical domains to recognize palindromic, double-stranded DNA.² A simple point mutation is enough to significantly hinder enzymatic activity and disrupt this dimer–dimer interaction. Biological activity is ultimately improved by this compatible alignment between a symmetric multimeric protein and a symmetric multimeric target.

While the example of *EcoRV* is one that naturally occurs, the idea of harnessing a symmetrical recognition mechanism can be adapted for synthetic systems, as we will demonstrate in this study with precision molecular recognition of the three-fold rotationally symmetric homotrimeric spike protein of the severe acute respiratory syndrome coronavirus 2 (SARS-CoV-2) virus³ by a branched homotrimeric DNA aptamer with three-fold rotational symmetry.

The SARS-CoV-2 virus and COVID-19 pandemic continue to pose a threat worldwide despite vaccination efforts.^{4–6} One

of the defining features of the virus is the spike (S) glycoprotein, which decorates the surface of the pathogen and mediates viral entry into the host cell.^{3,7} Although other SARS-CoV-2 proteins can potentially serve as antigen targets, several factors establish the S protein as a particularly useful target. Notably, its function is indispensable to the virus and its protruding nature offers the potential for detection without the need for lysis.^{3,8–11} Furthermore, the S protein is trimeric, possessing three identical monomers that arrange in a cyclical structure with three-fold rotational symmetry.^{3,8–11} This offers the opportunity to engineer compatible trimeric molecular recognition elements (MREs), capable of symmetrically recognizing multiple subunits of the same S protein.

An extensive array of MREs have been investigated for SARS-CoV-2 research since the onset of the pandemic.^{12–24} Among these MREs, nucleic acid aptamers have stood out as a

Received: September 15, 2022

Published: December 15, 2022



promising option.^{14–24} Aptamers are short, single-stranded oligonucleotides that demonstrate high binding affinity and selectivity toward a specific substrate.^{25–27} Their binding affinity can be further enhanced by creating multimeric aptamers by joining two or more monomeric substituents together, typically by linking monomers together in series to form a linear multimer.^{21,28–31} However, such an arrangement may result in one or more monomers being inaccessible to the target, particularly if the trimer is immobilized on a surface through a terminal end, as the innermost monomer closest to the surface would likely not be accessible for binding to the spike protein. Linear trimers may also be unable to align correctly with the three-fold symmetric spike protein, preventing the full enhancement of affinity. As an example, the affinity of the recently reported RBD-PB6 aptamer decreases from 129 nM for the monomer to 1.4 nM for the linear dimer, but then to only 0.8 nM for the linear trimer, suggesting an inability of the linear trimer to properly align with the binding sites on the trimeric spike protein.³¹

Herein, we report on the first branched trimeric aptamer, denoted as TMSA52, where each of the three aptamers is tethered to a central linker to produce a MRE with three-fold rotational symmetry, so that all three aptamers are equally accessible to and align with the subunits of the spike protein. Just as *EcoRV* binds symmetrically to palindromic sequences, the configuration of TMSA52 complements and structurally aligns with the trimeric nature of the S protein (Figure 1A). We show that TMSA52 binds several SARS-CoV-2 spike protein variants with picomolar affinity and diverse pseudotyped lentiviruses expressing SARS-CoV-2 spike protein variants with femtomolar affinity. We also describe a biosensor using TMSA52 in conjunction with Pd–Ir nanocubes (a

nanozyme), which was capable of sensitively detecting diverse pseudotyped lentiviruses in pooled human saliva with a limit of detection (LOD) as low as 6.3×10^3 cp/mL. The sensor performance was evaluated using 110 COVID-19-positive and COVID-19-negative saliva samples, providing sensitivity and specificity values of 84.0 and 98.3%, respectively, thus highlighting the potential of TMSA52 for the development of future rapid tests.

RESULTS AND DISCUSSION

Design of a Symmetric Homotrimeric Aptamer for the Trimeric Spike Protein of SARS-CoV-2. The aptamer used for this work is MSA52, a monomeric DNA aptamer (Figure 1B) discovered by us through selection with variant S proteins.²⁴ Impressively, MSA52 was found to universally recognize variants that were not analyzed in the original selection experiment, demonstrating that the aptamer is insensitive to emerging S protein mutations.²⁴ Hence, MSA52 is an ideal candidate for COVID-19 recognition, and the trimerization of this MRE should enhance its complementarity to and affinity for the S protein.

One intuitive method to combine the MSA52 monomers together is to make use of the chemical composition of trebler phosphoramidite.^{32,33} Trebler phosphoramidite has been widely used as a connector for the preparation of poly-labeled DNA probes since it is capable of being inserted into a DNA sequence as a nucleotide.^{32,33} With the use of a 15-thymine (T15) linker and DNA synthesizer, we harnessed the branched structural scaffold of a trebler to synthesize a DNA molecule containing three identical MSA52 sequences (Figure 1C), which is named TMSA52. Analysis with 10% denaturing polyacrylamide gel electrophoresis of chemically synthesized TMSA52 showed that TMSA52 was synthesized successfully in reference to monomeric and dimeric MSA52 sequences (Figure S1C). The choice of a T15 linker was made for the following reasons. First, MSA52 has been shown to bind to the receptor-binding domain (RBD) of the SARS-CoV-2 spike protein.^{16,24} Second, it has been demonstrated that the distance between RBD subunits on the spike protein trimer ranges from 2.7 to 7.4 nm,³⁴ considering the “closed” and “open” conformational states of the RBD. Third, our calculations indicate that each arm of the trebler-linked trimeric aptamer with a 15-thymine linker has a persistence length of 6.9 nm.³⁵ Due to the flexibility of trebler, the trimeric aptamer TMSA52 should allow for a fluctuation of aptamer distance from 0 to 12.0 nm (Figure S1, panels A and B), which completely covers the distance range among RBD subunits on each trimeric spike protein.

Assessment of Binding Affinity of TMSA52. Using a dot-blot assay,^{16,21,24} we first tested the binding affinity of TMSA52 (sequence listed in Table S1) for eight different SARS-CoV-2 spike protein variants, including the WT (Wild-Type), B.1.1.7 (Alpha), B.1.351 (Beta), P.1 (Gamma), B.1.429 (Epsilon), B.1.617.1 (Kappa), B.1.617.2 (Delta), and B.1.1.529 (Omicron) variants (Figure S2, panels A and B). After labeling with ³²P at the 5' end, TMSA52 was incubated with different concentrations of spike protein variants to form an aptamer/protein complex. The aptamer/protein complex was retained by a nitrocellulose membrane, while the free aptamer was collected on a nylon membrane. The concentration of the bound aptamer on the nitrocellulose membrane and unbound aptamer on the nylon membrane was determined by their radioactivity.

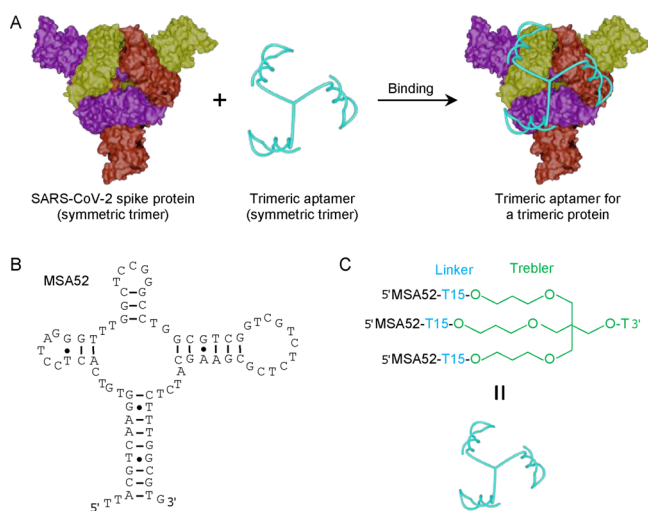


Figure 1. Design of a trimeric aptamer for the trimeric spike protein of SARS-CoV-2. (A) Top view of the SARS-CoV-2 trimeric spike protein showing the complementarity with the trimeric aptamer to achieve molecular recognition. The trimeric structure of the aptamer ligand complements the molecular scaffold of the spike protein and optimizes binding affinity. (B) Secondary structure of SARS-CoV-2 spike protein binding aptamer MSA52. The ability of MSA52 to universally identify ongoing and predicted SARS-CoV-2 variants of concern provides an ideal candidate for COVID-19 detection. (C) Construction of the trimeric aptamer with MSA52, trebler, and a 15-thymine linker. The trebler biomolecule enables the assembly of a symmetric, multimeric recognition element.

Figure 2A plots the bound fraction of aptamer against the concentrations of each spike protein variant. The dissociation

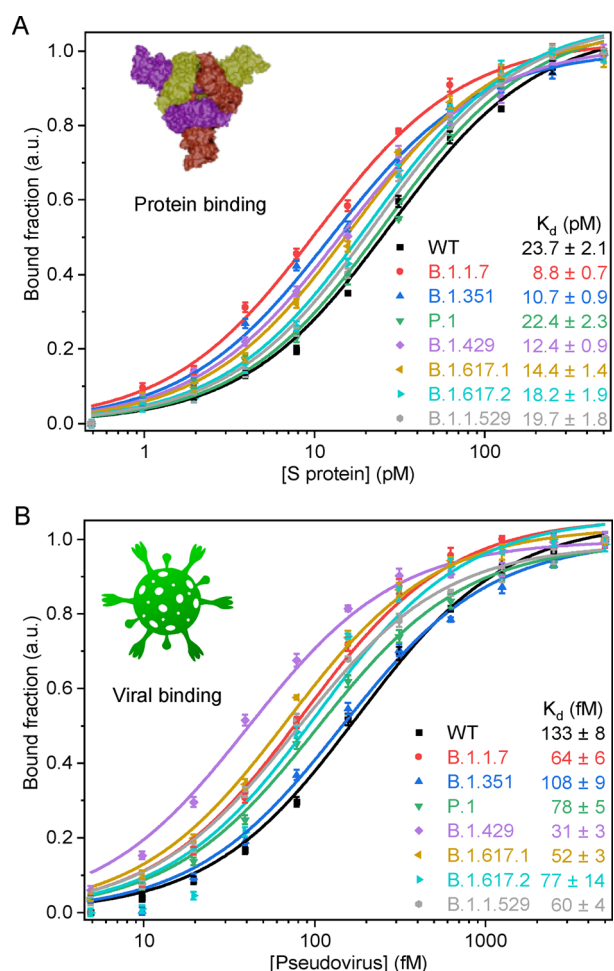


Figure 2. Assessment of binding affinity of TMSA52 for (A) SARS-CoV-2 spike protein variants and (B) pseudotyped lentiviruses displaying the spike protein variants. K_d values displayed consistently high affinity (pM to fM range) for both WT and variant strains.

constants (K_d values) were obtained via non-linear curve fitting using the equation $Y = B_{\max}X/(K_d + X)$, where Y refers to the bound fraction of the aptamer, B_{\max} represents the maximum bound fraction of the aptamer, and X stands for the concentration of spike proteins. The K_d values of TMSA52 for the eight spike protein variants ranged from 8.8 to 23.7 pM, which were approximately two orders of magnitude lower than those for the corresponding monomeric aptamer MSA52.²⁴ The significantly increased binding affinity was attributed to the superior trivalent interaction between the trimeric aptamer and the spike protein trimer.

TMSA52 was also tested for the binding of three control proteins including SARS-CoV-1 spike protein and spike RBD proteins of seasonal coronavirus 229E and OC43 (Figure S2, panels C and D). The K_d values for the control proteins exceeded 50 nM, demonstrating the highly specific recognition ability of TMSA52 for the SARS-CoV-2 spike proteins.

Following the same method, we next tested the binding affinities of TMSA52 for pseudotyped lentiviruses expressing the same spike protein variants, using a lentivirus without spike protein as a control (Figure S3, panels A–C). The bound fraction of TMSA52 was plotted against the concentration of

pseudoviruses to derive the K_d values (Figures 2B and S3D). The K_d values of TMSA52 for the eight pseudoviruses expressing different spike protein variants ranged from 31 to 133 fM, which was more than two orders of magnitude lower than those for the monomeric aptamer MSA52.²⁴ In contrast, the binding affinity for the control lentivirus was higher than 500 pM. Overall, the trimerization of MSA52 significantly increased the binding affinity for the recognition of all the SARS-CoV-2 spike protein variants. It is worth noting that previously reported linear dimeric or trimeric aptamers and circular dimeric aptamers developed for the SARS-CoV-2 spike protein achieved affinity enhancements of two orders of magnitude only for wild-type spike proteins, and only a one order of magnitude improvement for three spike protein variants, indicating that affinity improvements were not universal.^{19,21,31}

Cooperativity of Binding by Three Aptamer Arms.

The next logical step was to validate the cooperative effect among the aptamer arms of TMSA52 for the binding of spike protein. By blocking the arms of TMSA52 with a 40-nt antisense (AS) DNA molecule (Figure 3A), we can assess

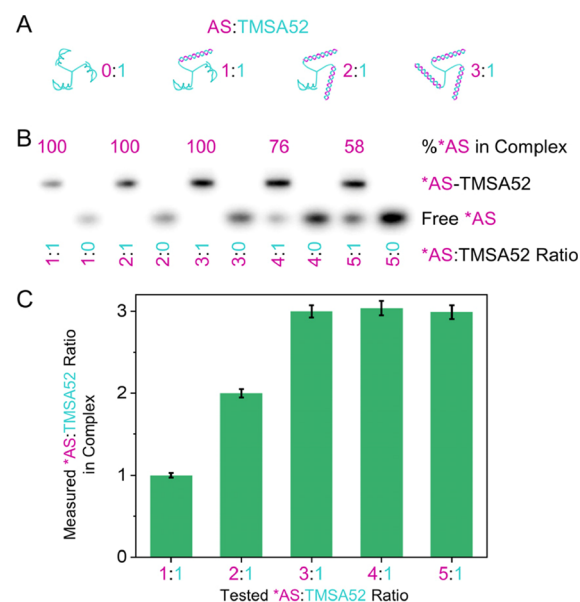


Figure 3. (A) Blocking of trimeric aptamer (TMSA52) arms using various AS:TMSA52 ratios. AS is a 40-nt single-stranded DNA sequence that is complementary to aptamer MSA52. (B) Electrophoretic mobility shift assay and (C) corresponding plot displaying the hybridization efficiency between ³²P-AS and TMSA52 at different AS:TMSA52 ratios.

whether all three aptamer arms are required for the best possible binding. The precise AS:TMSA52 ratios were determined by an electrophoretic mobility shift assay, which used radioactive AS labeled with ³²P at the 5' end. AS was mixed with TMSA52 in binding buffer at different ratios. After denaturation and annealing, the samples were analyzed by native polyacrylamide gel electrophoresis. As shown in Figure 3 (panels B and C), ³²P-AS hybridized efficiently with TMSA52, but reached saturation at a ³²P-AS to TMSA52 ratio of 3:1. Further increases of ³²P-AS concentration resulted in no increase of binding number since all three arms on each TMSA52 molecule are presumably at capacity.

We next investigated binding affinity of AS:TMSA52 complexes at different ratios for the spike protein. The B.1.1.529 variant spike protein was used for this experiment. The defined ratios of AS to ^{32}P -TMSA52 were mixed in binding buffer, followed by the addition of the B.1.1.529 spike protein. After a brief incubation at ambient temperature, the mixtures were analyzed by dot-blot assays. As shown in Figure 4 panels A and B, the binding activity of TMSA52 was

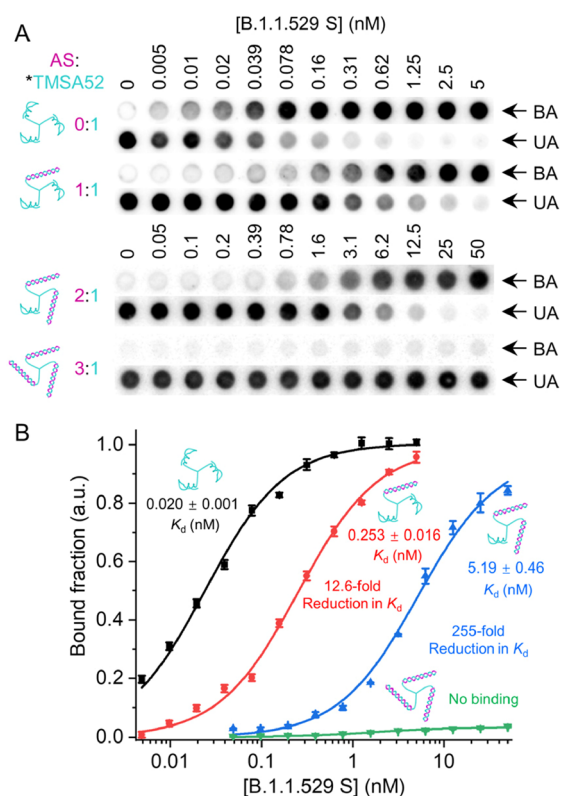


Figure 4. Cooperativity of binding by three aptamer arms. (A) Dot-blot assays and (B) corresponding binding affinity curves of TMSA52 for B.1.1.529 spike protein at different AS:TMSA52 ratios. BA: bound aptamer; UA: unbound aptamer.

gradually reduced by AS, with the K_d values increasing from 0.020 nM (AS:TMSA52 = 0:1) to 0.253 nM (AS:TMSA52 = 1:1) and 5.19 nM (AS:TMSA52 = 2:1). These values were consistent with the binding affinities of dimeric (DMSA52) and monomeric (MSA52) aptamers for the B.1.1.529 spike protein (Figure S4). When the AS:TMSA52 ratio reached 3:1, the binding affinity of TMSA52 for the spike protein was almost completely abolished. These results adequately demonstrate that three TMSA52 arms associate with the three spike protein subunits in a concerted fashion. These results are consistent with the improved binding affinity of spherical aptamers, icosahedral DNA nanocages, and net-shaped DNA nanostructures for SARS-CoV-2 spike protein.^{34,36–38}

Design of an ELABA. The universal recognition of spike variants by TMSA52 offers a solution to a significant COVID-19 complication—the continuing emergence of variants of concern. These variants have significantly hindered the sensitivity of current antigen-based rapid tests and increased the need for continuous adjustments with novel MREs.^{39,40} TMSA52 offers a promising breakthrough in COVID-19

detection, as it has been proven to recognize a vast array of SARS-CoV-2 variants.

To employ the trimeric aptamer for the detection of all SARS-CoV-2 variants in an easy, lab-ready format, we chose to utilize a sandwich assay employing nanozymes, entities known for their high peroxidase-mimicking activity (Figure 5A). Nanozymes are popular candidates to provide colorimetric signal outputs and greatly improve detection sensitivity.⁴¹ Thus far, the nanozymes with the highest peroxidase-mimicking activity are Pd–Ir nanocubes, which display approximately three orders of magnitude higher catalytic activity than horseradish peroxidase.^{41–43} To conduct an enzyme-linked aptamer binding assay (ELABA), a biotinylated trimeric aptamer (TMSA52-B, Table S1) was first attached to a streptavidin-coated microtiter plate or Pd–Ir nanocubes (synthesized according to our previously reported methods; see Figure S5.^{42,43}) through the biotin/streptavidin interaction, which is one of the strongest biomolecular interactions.⁴⁴ SARS-CoV-2 pseudovirus was then added to the aptamer-conjugated microtiter plate to bind with the immobilized trimeric aptamer. After washing, aptamer-conjugated Pd–Ir nanocubes were introduced to bind with the pseudovirus captured on the plate. The presence of SARS-CoV-2 pseudovirus variants leads to the immobilization of aptamer-conjugated Pd–Ir nanocubes through a sandwich structure, which efficiently catalyzes the oxidation of colorless TMB with H_2O_2 to generate blue oxidized products. H_2SO_4 is then used to convert the TMB from blue to yellow. The concentration of the pseudovirus, which is proportional to the absorbance at 450 nm, can be easily determined by a plate reader.

Using B.1.1.529 pseudovirus as a model target, the detection performances of trimeric (TMSA52-B), dimeric (DMSA52-B), and monomeric (MSA52-B) aptamer-based assays were compared. The ELABA procedures for dimeric and monomeric aptamers were the same as the above-described procedures for the trimeric aptamer, except for the substitution of TMSA52-B with DMSA52-B or MSA52-B. As shown in Figure S6, the yellow intensity and absorbance at 450 nm increased proportionally with the concentration of the B.1.1.529 pseudovirus. The TMSA52-based method displayed a detection limit of 6.5×10^3 cp/mL, which was 7.1-fold lower than DMSA52 (LOD 4.7×10^4 cp/mL, based on 3-fold standard deviation of blank samples) and 126-fold lower than MSA52 (LOD 8.2×10^5 cp/mL). The results demonstrate a significant improvement for the detection of pseudovirus by the trimerization of the original MSA52 aptamer.

To further verify the importance of trimeric binding for sensitive detection, AS was introduced to block the arms of TMSA52 prior to colorimetric detection. As shown in Figure 5 panels B and C, the detection limit of the TMSA52-based assay increased from 6.5×10^3 to 4.8×10^4 cp/mL and subsequently to 8.5×10^5 cp/mL with the blocking of one and two TMSA52 arms, respectively. The results of increasing the AS:TMSA52 ratio were consistent with the DMSA52 and MSA52-based assays (Figure S6), demonstrating the importance of trimerization for enhancing the performance of biosensing assays.

Afterward, the specificity of the TMSA52-based assay for the detection of B.1.1.529 pseudoviruses was tested. SARS-CoV-1 spike, spike RBD of seasonal coronaviruses 229E and OC43, human IgG, amylase, BSA, and lentivirus were used as controls. The concentrations of control protein (10 nM) were approximately 5 orders of magnitude higher than B.1.1.529

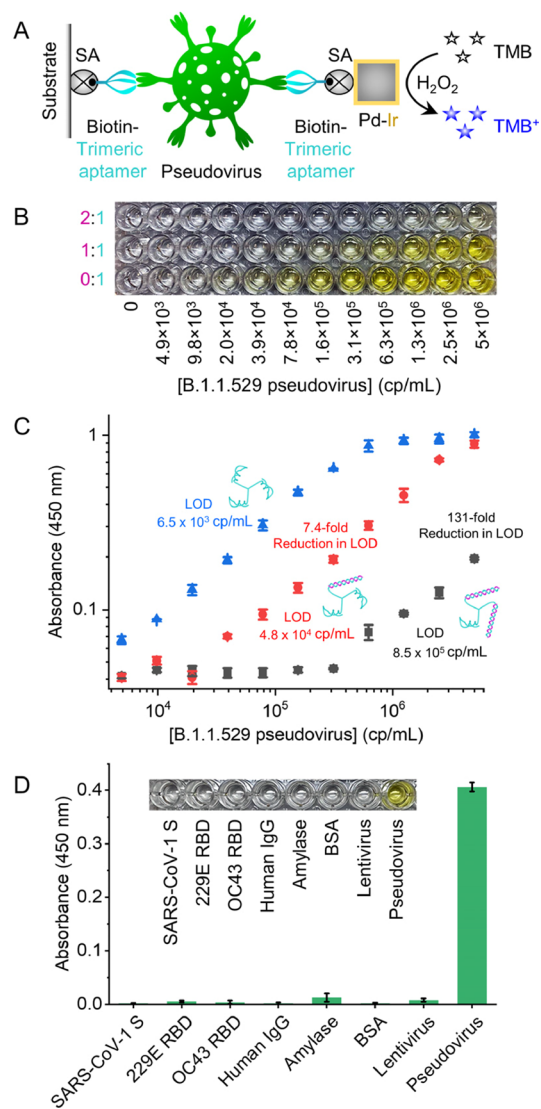


Figure 5. Design of an enzyme-linked aptamer binding assay for colorimetric detection of SARS-CoV-2 using TMSA52. (A) Illustration of colorimetric sandwich assay in which SARS-CoV-2 pseudoviruses are captured with biotinylated aptamers, using Pd–Ir nanocubes as peroxidase-mimicking nanozymes; SA: streptavidin. (B) Photograph of the colorimetric test and (C) corresponding concentration–response plots using A_{450} for pseudotyped lentivirus expressing the SARS-CoV-2 B.1.1.529 spike protein in buffer, using the biotinylated trimeric aptamer (TMSA52-B) at different AS:TMSA52-B ratios; AS is a 40-nt single-stranded DNA sequence that is complementary to aptamer MSA52. (D) Response based on A_{450} (inset: photograph) demonstrating the specificity of the trimeric aptamer-based method for the detection of B.1.1.529 pseudovirus. SARS-CoV-1 spike protein, spike RBD of seasonal coronaviruses 229E and OC43, human IgG, amylase, BSA, and lentivirus are used as controls. The concentrations of control proteins were 10 nM; the concentrations of pseudovirus and lentivirus were 10^5 cp/mL (corresponding to 120 aM). LOD: limit of detection, 3 times the standard deviation of blank samples.

pseudoviruses (120 fM). As shown in Figure 5D, the assay was capable of specifically detecting B.1.1.529 pseudoviruses with a negligible signal response for the control proteins or lentivirus. These results strongly support the practicality of TMSA52 as a COVID-19 MRE as demonstrated by its exceptional binding affinity and specificity.

Detection of Pseudoviruses Spiked in Human Saliva.

We next employed the TMSA52-based biosensor for the detection of eight SARS-CoV-2 spike variant pseudoviruses spiked in 25% pooled human saliva. Once again, the yellow intensity and absorbance at 450 nm increased proportionally with the pseudovirus concentration (Figure 6). The LOD

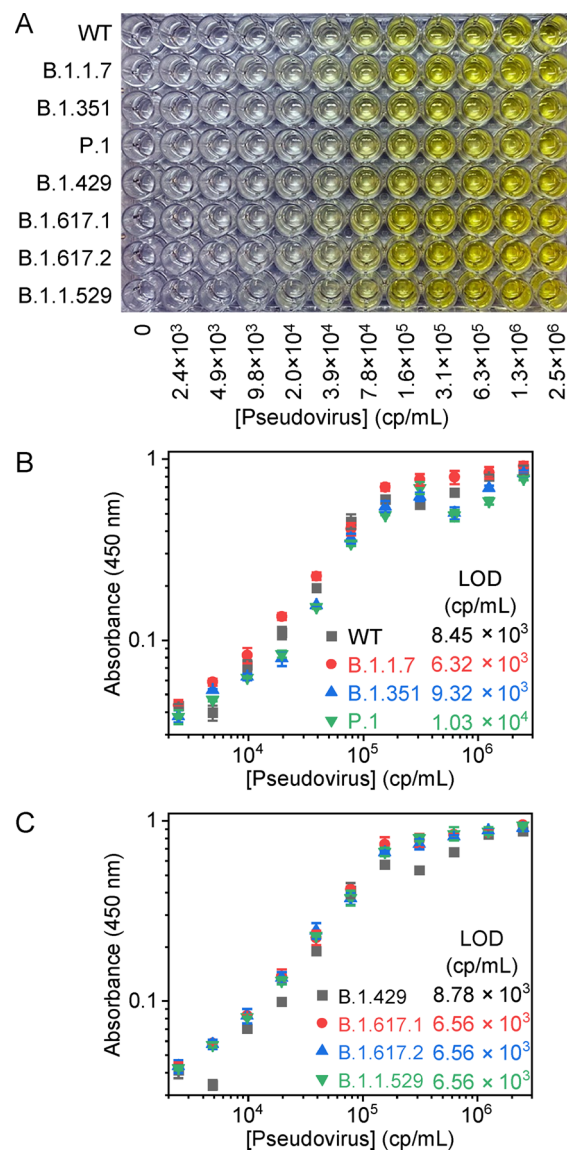


Figure 6. Detection of pseudoviruses spiked into human saliva. (A) Photograph of the colorimetric test and (B and C) corresponding plots depicting the detection of pseudoviruses expressing different spike protein variants spiked in pooled human saliva using the ELABA assay with TMSA52. LOD: limit of detection, 3 times the standard deviation of blank samples.

ranged between 6.3×10^3 and 1.0×10^4 cp/mL for all eight pseudovirus variants, with the highest detection sensitivity for the B.1.1.7 variant and the lowest detection sensitivity for the P.1 variant. These results highlight the universal recognition capabilities of the TMSA52 aptamer.

Evaluation of the Biosensor Using Clinical Samples.

To evaluate the clinical utility of the sandwich assay employing the trimeric aptamer, we examined a panel of 110 patient saliva samples, including 50 nasopharyngeal swab (NPS)-positive and 60 NPS-negative samples. Table S2 provides details on

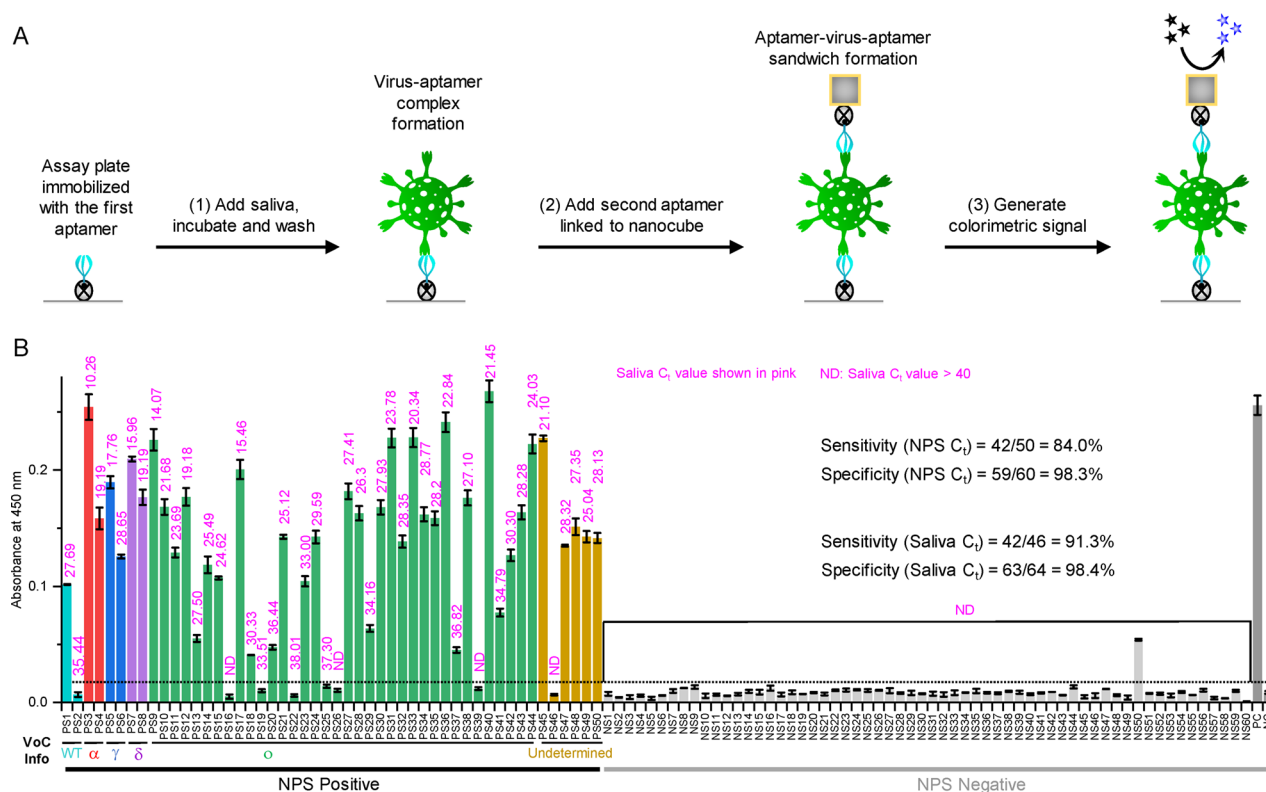


Figure 7. Clinical evaluation of the trimeric aptamer assay. (A) Schematic illustration and (B) signal response of the TMSA52-based ELABA for the detection SARS-CoV-2 in clinical saliva samples, including 50 NPS-positive samples [cyan, red, blue, purple, green, and mustard yellow refer to wild-type SARS-CoV-2, Alpha (B.1.1.7), Gamma (P.1), Delta (B.1.617.2), Omicron (B.1.1.529: PS9-PS21, BA.2: PS22-PS23, BA.4: PS24-PS26, BA.5: PS27-PS36, and BA.2.12.1: PS37-PS44) and undetermined variants, respectively] and 60 NPS-negative samples (gray). PS: positive saliva sample; NS: negative saliva sample; PC: positive control, 4×10^4 cp/mL B.1.1.529 pseudovirus spiked in commercial pooled human saliva; NC: negative control, commercial pooled human saliva. The dotted line marks the cut-off point for the TMSA52-based assay. The error bars stand for the standard deviation of three ($n = 3$) replicated samples. ND: not detected. NPS: nasopharyngeal swab.

each sample, including NPS and saliva-based C_t values obtained from reverse transcription-polymerase chain reaction (RT-PCR) along with the presumed variant (for positive samples). Figure 7A shows the assay workflow. TMSA52-B was first immobilized to the surface of the microwell. Saliva samples were diluted to 25% using assay buffer and then incubated with the TMSA52-B aptamer (30 min), followed by a washing step to capture the virus on the microwell surface. The detection TMSA52-B aptamer, prebound to Pd–Ir nanoplates, was then added and allowed to incubate for 30 min prior to washing. TMB was then added, and the signal was measured after 10 min. The total sample to readout time was 70 min. However, high throughput analysis can be achieved using a 96-well plate or 384-well plate.

Figure 7B shows the absorbance values measured for each of the individual positive (PS#) and negative (NS#) saliva samples, along with high (PC) and low (NC) controls. The C_t value for each positive saliva sample is shown above its respective bar. A plot of C_t values against absorbance at 450 nm showed an inversely proportional relationship (Figure S7A), with an R -squared (R^2) value of 0.752. It demonstrates a good consistency between RT-PCR and TMSA52-based ELABA. Based on a box and whisker plot (Figure S7B) and a receiver operating characteristic curve (Figure S7C), we determined the clinical cut-off absorbance (A_{450}) value to be 0.027, which resulted in a sensitivity of 84.0% true positives detected, a specificity of 98.3% true negatives detected, and an overall accuracy of 92.9%. We note that while each of the eight

misidentified samples was identified as positive using RT-PCR of NPS samples (though all with C_t values over 33), four of these samples did not show detectable RNA in the corresponding saliva sample; hence the clinical sensitivity based on a comparison to saliva RT-PCR data rises to 91.3% if these four samples are considered as negatives.

An important point from Figure 7B is that the detection of SARS-CoV-2 in positive patient saliva does not depend on the variant. This clearly shows the key advantage of using the TMSA52 aptamer, as it can produce positive signals regardless of the variant. The data also show that negative patient saliva samples do not contribute to significant background signals. This further supports the high selectivity of the TMSA52 aptamer, as it is insensitive to potential interferents that might be present in patient saliva. As a comparison, the 110 patient saliva samples were also tested using the BTNX Rapid Response COVID-19 rapid antigen test. As shown in Figure S8, the rapid test showed a detection sensitivity (NPS) of 72%, which was lower than the TMSA52-based ELABA method.

CONCLUSIONS

We have described the most optimal aptamer thus far for SARS-CoV-2 recognition. To engineer our novel MRE, we adopted a trebler and linker system, while utilizing our pre-existing, universal aptamer MSAS2. TMSA52 can recognize the most notable spike protein variants, including the wild-type, B.1.1.7 (Alpha), B.1.351 (Beta), P.1 (Gamma), B.1.429 (Epsilon), B.1.617.1 (Kappa), B.1.617.2 (Delta), and recent

B.1.1.529 (Omicron) variants, with K_d values ranging from 8.8 to 23.7 pM. Compared to its monomeric and dimeric equivalents, TMSA52 exhibited increased binding affinity toward both the S protein and pseudovirus samples. The exceptional recognition was attributed to the symmetrical, multivalent interaction between the trimeric aptamer and spike protein trimer. For the application of our aptamer into a practical setting, we developed a colorimetric assay for the detection of SARS-CoV-2 variants using Pd–Ir nanocubes as peroxidase mimicking nanozymes for the signal output. Eight pseudoviruses displaying different SARS-CoV-2 spike variants in pooled human saliva have been specifically identified with detection limits ranging from 6.3×10^3 to 1.0×10^4 cp/mL. Finally, the assay was applied to the detection of SARS-CoV-2 in patient saliva samples, providing a clinical sensitivity of 84.0% and specificity of 98.3% compared to RT-PCR of NPS samples.

We were ultimately able to build upon the foundation of our published SARS-CoV-2 aptamers for the development of TMSA52. Even though we previously reported on a universal aptamer that could recognize multiple variants, we had yet to take advantage of the structural scaffold of our target. The trimeric aptamer shape is a perfect fit for the trimeric S protein, granting it an affinity and specificity that is unique relative to any other aptamer published in the literature. TMSA52 holds great potential for broader diagnostic and therapeutic COVID-19 applications and, moving forward, should serve as the dominant choice of all SARS-CoV-2 MREs.

Furthermore, given the symmetrical nature of viruses and their coat proteins, there is reason to suggest that our multimeric aptamer strategy can be generalized and adopted to other pathogens. Outer coat proteins, such as hemagglutinin of influenza and encoded envelope glycoprotein of herpes simplex virus, also arrange in a homomer-like fashion.^{45,46} Therefore, continuing this strategy of symmetric and multimeric aptamer assembly is paramount for viral recognition. This approach, in fact, would be no different from the one employed by our own immune system. A specific ubiquitin ligase, known as TRIM5, is an immune protein that detects and inhibits retroviruses. Interestingly, TRIM5 must connect into a symmetrical trimer to recognize a symmetrical viral coat protein, which ultimately triggers ubiquitination and inflammatory support.⁴⁷ Again, while the mechanisms of EcoRV or TRIM5 naturally occur in biology, their symmetric and multimeric approaches can be emulated in aptamers. This will provide a new method for engineering high performing MREs for a wide range of target molecules.

■ ASSOCIATED CONTENT

SI Supporting Information

The Supporting Information is available free of charge at <https://pubs.acs.org/doi/10.1021/jacs.2c09870>.

Experimental procedures; characterization of TMSA52 size; dot blot assay for spike protein and pseudovirus; TEM characterization of Pd–Ir nanocubes; monomeric, dimeric, and trimeric aptamer-based ELABA; and receiver operating characteristics curve analysis (PDF)

■ AUTHOR INFORMATION

Corresponding Authors

John D. Brennan – *Biointerfaces Institute, McMaster University, Hamilton, Ontario L8S 4O3, Canada;*

orcid.org/0000-0003-3461-9824; Email: brennanj@mcmaster.ca

Yingfu Li – *Department of Biochemistry and Biomedical Sciences and Michael G. DeGroot Institute of Infectious Disease Research, McMaster University, Hamilton, Ontario L8S 4K1, Canada; Biointerfaces Institute, McMaster University, Hamilton, Ontario L8S 4O3, Canada; School of Biomedical Engineering, Hamilton, Ontario L8S 4K1, Canada; orcid.org/0000-0002-7533-6743; Email: liyong@mcmaster.ca*

Authors

Jiuxing Li – *Department of Biochemistry and Biomedical Sciences, McMaster University, Hamilton, Ontario L8S 4K1, Canada*

Zijie Zhang – *Department of Biochemistry and Biomedical Sciences, McMaster University, Hamilton, Ontario L8S 4K1, Canada*

Jimmy Gu – *Department of Biochemistry and Biomedical Sciences, McMaster University, Hamilton, Ontario L8S 4K1, Canada*

Ryan Amini – *Department of Biochemistry and Biomedical Sciences, McMaster University, Hamilton, Ontario L8S 4K1, Canada*

Alexandria G. Mansfield – *Department of Biochemistry and Biomedical Sciences, McMaster University, Hamilton, Ontario L8S 4K1, Canada*

Jianrun Xia – *Department of Biochemistry and Biomedical Sciences, McMaster University, Hamilton, Ontario L8S 4K1, Canada*

Dawn White – *Biointerfaces Institute, McMaster University, Hamilton, Ontario L8S 4O3, Canada*

Hannah D. Stacey – *Department of Biochemistry and Biomedical Sciences, Michael G. DeGroot Institute of Infectious Disease Research, and McMaster Immunology Research Centre, McMaster University, Hamilton, Ontario L8S 4K1, Canada*

Jann C. Ang – *Department of Biochemistry and Biomedical Sciences, Michael G. DeGroot Institute of Infectious Disease Research, and McMaster Immunology Research Centre, McMaster University, Hamilton, Ontario L8S 4K1, Canada*

Gurpreet Panesar – *Department of Biochemistry and Biomedical Sciences, McMaster University, Hamilton, Ontario L8S 4K1, Canada*

Alfredo Capretta – *Biointerfaces Institute, McMaster University, Hamilton, Ontario L8S 4O3, Canada; Michael G. DeGroot Institute of Infectious Disease Research, McMaster University, Hamilton, Ontario L8S 4K1, Canada*

Carlos D. M. Filipe – *Department of Chemical Engineering, McMaster University, Hamilton, Ontario L8S 4K1, Canada; orcid.org/0000-0002-7410-3323*

Karen Mossman – *McMaster Immunology Research Centre and Department of Medicine, McMaster University, Hamilton, Ontario L8S 4K1, Canada*

Bruno J. Salena – *Department of Medicine, McMaster University, Hamilton, Ontario L8S 4K1, Canada*

Jonathan B. Gubbay – *Public Health Ontario Laboratory, Toronto, Ontario M5G 1M1, Canada*

Cynthia Balion – *Department of Pathology and Molecular Medicine, McMaster University, Hamilton, Ontario L8S 4K1, Canada*

Leyla Soleymani – *Michael G. DeGroot Institute of Infectious Disease Research and Department of Engineering Physics,*

McMaster University, Hamilton, Ontario L8S 4K1, Canada; School of Biomedical Engineering, Hamilton, Ontario L8S 4K1, Canada; orcid.org/0000-0003-4915-2999

Matthew S. Miller – Department of Biochemistry and Biomedical Sciences, Michael G. DeGroot Institute of Infectious Disease Research, and McMaster Immunology Research Centre, McMaster University, Hamilton, Ontario L8S 4K1, Canada

Deborah Yamamura – Michael G. DeGroot Institute of Infectious Disease Research and Department of Pathology and Molecular Medicine, McMaster University, Hamilton, Ontario L8S 4K1, Canada

Complete contact information is available at:

<https://pubs.acs.org/10.1021/jacs.2c09870>

Author Contributions

The manuscript was written through contributions of all authors.

Notes

The authors declare no competing financial interest.

ACKNOWLEDGMENTS

This work was supported by funding from Canadian Institutes of Health Research (CIHR), Natural Sciences and Engineering Research Council of Canada (NSERC), Canada Foundation for Innovation (CFI), and the Ministry for Research and Innovation (MRI) of Ontario. J.D.B. holds the Canada Research Chair in Point-of-Care Diagnostics.

REFERENCES

- (1) Siggers, T.; Gordán, R. Protein–DNA binding: complexities and multi-protein codes. *Nucleic Acids Res.* **2014**, *42*, 2099–2111.
- (2) Stahl, F.; Wende, W.; Jeltsch, A.; Pingoud, A. Introduction of asymmetry in the naturally symmetric restriction endonuclease EcoRV to investigate intersubunit communication in the homodimeric protein. *Proc. Natl. Acad. Sci. U. S. A.* **1996**, *93*, 6175–6180.
- (3) Walls, A. C.; Park, Y.-J.; Tortorici, M. A.; Wall, A.; McGuire, A. T.; Velesler, D. Structure, function, and antigenicity of the SARS-CoV-2 spike glycoprotein. *Cell* **2020**, *181*, 281–292.e6.
- (4) Struyf, T.; Deeks, J. J.; Dinnes, J.; Takwoingi, Y.; Davenport, C.; Leeflang, M. M.; Spijker, R.; Hooft, L.; Emperador, D.; Domen, J. Signs and symptoms to determine if a patient presenting in primary care or hospital outpatient settings has COVID-19. *Cochrane Database Syst. Rev.* **2022**, *7*, CD013665.
- (5) Yu, J.; Collier, A.-R. Y.; Rowe, M.; Mardas, F.; Ventura, J. D.; Wan, H.; Miller, J.; Powers, O.; Chung, B.; Siamatu, M. Neutralization of the SARS-CoV-2 Omicron BA.1 and BA.2 variants. *N. Engl. J. Med.* **2022**, *386*, 1579–1580.
- (6) Tegally, H.; Moir, M.; Everatt, J.; Giovanetti, M.; Scheepers, C.; Wilkinson, E.; Subramoney, K.; Makatini, Z.; Moyo, S.; Amoako, D. G.; Baxter, C.; Althaus, C. L.; Anyaneji, U. J.; Kekana, D.; Viana, R.; Giandhari, J.; Lessells, R. J.; Maponga, T.; Maruapula, D.; Choga, W.; Matshaba, M.; Mbulawa, M. B.; Msomi, N.; NGS-SA consortium; Bester, A. P.; Claassen, M.; Doolabh, D.; Mudau, I.; Mbhele, N.; Engelbrecht, S.; Goedhals, D.; Hardie, D.; Hsiao, N. Y.; Iranzadeh, A.; Ismail, A.; Joseph, R.; Maharaj, A.; Mahlangu, B.; Mahlakwane, K.; Davis, A.; Marais, G.; Mlisana, K.; Mnguni, A.; Mohale, T.; Motsatsi, G.; Mwangi, P.; Ntuli, N.; Nyaga, M.; Olubayo, L.; Radibe, B.; Ramphal, Y.; Ramphal, U.; Strasheim, W.; Tebeila, N.; van Wyk, S.; Wilson, S.; Lucaci, A. G.; Weaver, S.; Maharaj, A.; Pillay, Y.; Davids, M.; Mendes, A.; Mayaphi, S.; Naidoo, Y.; Pillay, S.; Sanko, T. J.; San, J. E.; Scott, L.; Singh, L.; Magini, N. A.; Smith-Lawrence, P.; Stevens, W.; Dor, G.; Tshiabula, D.; Wolter, N.; Preiser, W.; Treurnicht, F. K.; Venter, M.; Chiloane, G.; McIntyre, C.; O’Toole, A.; Ruis, C.; Peacock, T. P.; Roemer, C.; Kosakovsky Pond, S. L.; Williamson, C.;

Pybus, O. G.; Bhiman, J. N.; Glass, A.; Martin, D. P.; Jackson, B.; Rambaut, A.; Laguda-Akingba, O.; Gaseitsiwe, S.; von Gottberg, A.; de Oliveira, T. Emergence of SARS-CoV-2 Omicron lineages BA.4 and BA.5 in South Africa. *Nat. Med.* **2022**, *28*, 1785–1790.

(7) Berry, J. D.; Jones, S.; Drebot, M. A.; Andonov, A.; Sabara, M.; Yuan, X. Y.; Weingartl, H.; Fernando, L.; Marszal, P.; Gren, J.; Nicolas, B.; Andonova, M.; Ranada, F.; Gubbins, M. J.; Ball, T. B.; Kitching, P.; Li, Y.; Kabani, A.; Plummer, F. Development and characterisation of neutralising monoclonal antibody to the SARS-coronavirus. *J. Virol. Methods* **2004**, *120*, 87–96.

(8) Plante, J. A.; Liu, Y.; Liu, J.; Xia, H.; Johnson, B. A.; Lokugamage, K. G.; Zhang, X.; Muruato, A. E.; Zou, J.; Fontes-Garfias, C. R.; Mirchandani, D.; Scharf, D.; Billelo, J. P.; Ku, Z.; An, Z.; Kalveram, B.; Freiberg, A. N.; Menachery, V. D.; Xie, X.; Plante, K. S.; Weaver, S. C.; Shi, P. Y. Spike mutation D614G alters SARS-CoV-2 fitness. *Nature* **2021**, *592*, 116–121.

(9) Henderson, R.; Edwards, R. J.; Mansouri, K.; Janowska, K.; Stalls, V.; Gobeil, S.; Kopp, M.; Li, D.; Parks, R.; Hsu, A. L.; Borgnia, M. J.; Haynes, B. F.; Acharya, P. Controlling the SARS-CoV-2 spike glycoprotein conformation. *Nat. Struct. Mol. Biol.* **2020**, *27*, 925–933.

(10) Cai, Y.; Zhang, J.; Xiao, T.; Peng, H.; Sterling, S. M.; Walsh, R. M., Jr.; Rawson, S.; Rits-Volloch, S.; Chen, B. Distinct conformational states of SARS-CoV-2 spike protein. *Science* **2020**, *369*, 1586–1592.

(11) Yurkovetskiy, L.; Wang, X.; Pascal, K. E.; Tomkins-Tinch, C.; Nyalile, T. P.; Wang, Y.; Baum, A.; Diehl, W. E.; Dauphin, A.; Carbone, C.; Veinotte, K.; Egri, S. B.; Schaffner, S. F.; Lemieux, J. E.; Munro, J. B.; Rafique, A.; Barve, A.; Sabeti, P. C.; Kyratsous, C. A.; Dudkina, N. V.; Shen, K.; Luban, J. Structural and functional analysis of the D614G SARS-CoV-2 spike protein variant. *Cell* **2020**, *183*, 739–751.

(12) Theel, E. S.; Slev, P.; Wheeler, S.; Couturier, M. R.; Wong, S. J.; Kadkhoda, K. The role of antibody testing for SARS-CoV-2: is there one? *J. Clin. Microbiol.* **2020**, *58*, e00797-20.

(13) Lee, W. S.; Wheatley, A. K.; Kent, S. J.; DeKosky, B. J. Antibody-dependent enhancement and SARS-CoV-2 vaccines and therapies. *Nat. Microbiol.* **2020**, *5*, 1185–1191.

(14) Song, Y.; Song, J.; Wei, X.; Huang, M.; Sun, M.; Zhu, L.; Lin, B.; Shen, H.; Zhu, Z.; Yang, C. Discovery of aptamers targeting the receptor-binding domain of the SARS-CoV-2 spike glycoprotein. *Anal. Chem.* **2020**, *92*, 9895–9900.

(15) Kacherovsky, N.; Yang, L. F.; Dang, H. V.; Cheng, E. L.; Cardle, I. I.; Walls, A. C.; McCallum, M.; Sellers, D. L.; DiMaio, F.; Salipante, S. J.; Corti, D.; Velesler, D.; Pun, S. H. Discovery and characterization of spike N-terminal domain-binding aptamers for rapid SARS-CoV-2 detection. *Angew. Chem., Int. Ed.* **2021**, *60*, 21211–21215.

(16) Li, J.; Zhang, Z.; Gu, J.; Stacey, H. D.; Ang, J. C.; Capretta, A.; Filipe, C. D.; Mossman, K. L.; Balion, C.; Salena, B. J.; Yamamura, D.; Soleymani, L.; Miller, M. S.; Brennan, J. D.; Li, Y. Diverse high-affinity DNA aptamers for wild-type and B.1.1.7 SARS-CoV-2 spike proteins from a pre-structured DNA library. *Nucleic Acids Res.* **2021**, *49*, 7267–7279.

(17) Liu, X.; Wang, Y. L.; Wu, J.; Qi, J.; Zeng, Z.; Wan, Q.; Chen, Z.; Manandhar, P.; Cavener, V. S.; Boyle, N. R.; Fu, X.; Salazar, E.; Kuchipudi, S. V.; Kapur, V.; Zhang, X.; Umetani, M.; Sen, M.; Willson, R. C.; Chen, S. H.; Zu, Y. Neutralizing aptamers block S/RBD-ACE2 interactions and prevent host cell infection. *Angew. Chem., Int. Ed.* **2021**, *60*, 10273–10278.

(18) Schmitz, A.; Weber, A.; Bayin, M.; Breuers, S.; Fieberg, V.; Famulok, M.; Mayer, G. A SARS-CoV-2 spike binding DNA aptamer that inhibits pseudovirus infection by an RBD-independent mechanism. *Angew. Chem., Int. Ed.* **2021**, *60*, 10279–10285.

(19) Sun, M.; Liu, S.; Wei, X.; Wan, S.; Huang, M.; Song, T.; Lu, Y.; Weng, X.; Lin, Z.; Chen, H.; Song, Y.; Yang, C. Aptamer blocking strategy inhibits SARS-CoV-2 virus infection. *Angew. Chem., Int. Ed.* **2021**, *60*, 10266–10272.

(20) Yang, G.; Li, Z.; Mohammed, I.; Zhao, L.; Wei, W.; Xiao, H.; Guo, W.; Zhao, Y.; Qu, F.; Huang, Y. Identification of SARS-CoV-2 against aptamer with high neutralization activity by blocking the RBD

- domain of spike protein 1. *Signal Transduct. Target. Ther.* **2021**, *6*, 227.
- (21) Zhang, Z.; Pandey, R.; Li, J.; Gu, J.; White, D.; Stacey, H. D.; Ang, J. C.; Steinberg, C. J.; Capretta, A.; Filipe, C. D.; Mossman, K.; Balion, C.; Miller, M. S.; Salena, B. J.; Yamamura, D.; Soleymani, L.; Brennan, J. D.; Li, Y. High-affinity dimeric aptamers enable the rapid electrochemical detection of wild-type and B.1.1.7 SARS-CoV-2 in unprocessed saliva. *Angew. Chem., Int. Ed.* **2021**, *60*, 24266–24274.
- (22) Amini, R.; Zhang, Z.; Li, J.; Gu, J.; Brennan, J.; Li, Y. Aptamers for SARS-CoV-2: isolation, characterization, and diagnostic and therapeutic developments. *Anal. Sens.* **2022**, e202200012.
- (23) Li, J.; Zhang, Z.; Amini, R.; Li, Y. One solution for all: searching for universal aptamers for constantly mutating spike proteins of SARS-CoV-2. *ChemMedChem* **2022**, *17*, e202200166.
- (24) Zhang, Z.; Li, J.; Gu, J.; Amini, R.; Stacey, H.; Ang, J.; White, D.; Filipe, C.; Mossman, K.; Miller, M. A universal DNA aptamer that recognizes spike proteins of diverse SARS-CoV-2 variants of concern. *Chem. – Eur. J.* **2022**, *28*, e202200078.
- (25) Song, S.; Wang, L.; Li, J.; Fan, C.; Zhao, J. Aptamer-based biosensors. *TrAC, Trends Anal. Chem.* **2008**, *27*, 108–117.
- (26) McConnell, E. M.; Nguyen, J.; Li, Y. Aptamer-based biosensors for environmental monitoring. *Front. Chem.* **2020**, *8*, 434.
- (27) Navani, N. K.; Li, Y. Nucleic acid aptamers and enzymes as sensors. *Curr. Opin. Chem. Biol.* **2006**, *10*, 272–281.
- (28) Manochehry, S.; McConnell, E. M.; Li, Y. Unraveling determinants of affinity enhancement in dimeric aptamers for a dimeric protein. *Sci. Rep.* **2019**, *9*, 17824.
- (29) Riccardi, C.; Napolitano, E.; Musumeci, D.; Montesarchio, D. Dimeric and multimeric DNA aptamers for highly effective protein recognition. *Molecules* **2020**, *25*, 5227.
- (30) Di Giusto, D. A.; King, G. C. Construction, stability, and activity of multivalent circular anticoagulant aptamers. *J. Biol. Chem.* **2004**, *279*, 46483–46489.
- (31) Valero, J.; Civit, L.; Dupont, D. M.; Selnhin, D.; Reinert, L. S.; Idorn, M.; Israels, B. A.; Bednarz, A. M.; Bus, C.; Asbach, B.; Peterhoff, D.; Pedersen, F. S.; Birkedal, V.; Wagner, R.; Paludan, S. R.; Kjems, J. A serum-stable RNA aptamer specific for SARS-CoV-2 neutralizes viral entry. *Proc. Natl. Acad. Sci. U. S. A.* **2021**, *118*, e2112942118.
- (32) Shchepinov, M.; Udalova, I.; Bridgman, A.; Southern, E. Oligonucleotide dendrimers: synthesis and use as polylabelled DNA probes. *Nucleic Acids Res.* **1997**, *25*, 4447–4454.
- (33) Shchepinov, M. S.; Mir, K. U.; Elder, J. K.; Frank-Kamenetskii, M. D.; Southern, E. M. Oligonucleotide dendrimers: stable nanostructures. *Nucleic Acids Res.* **1999**, *27*, 3035–3041.
- (34) Zhang, J.; Xu, Y.; Huang, Y.; Sun, M.; Liu, S.; Wan, S.; Chen, H.; Yang, C.; Yang, Y.; Song, Y. Spatially patterned neutralizing icosahedral DNA nanocage for efficient SARS-CoV-2 blocking. *J. Am. Chem. Soc.* **2022**, *144*, 13146–13153.
- (35) Murphy, M.; Rasnik, I.; Cheng, W.; Lohman, T. M.; Ha, T. Probing single-stranded DNA conformational flexibility using fluorescence spectroscopy. *Biophys. J.* **2004**, *86*, 2530–2537.
- (36) Sun, M.; Liu, S.; Song, T.; Chen, F.; Zhang, J.; Huang, J.-A.; Wan, S.; Lu, Y.; Chen, H.; Tan, W. Spherical neutralizing aptamer inhibits SARS-CoV-2 infection and suppresses mutational escape. *J. Am. Chem. Soc.* **2021**, *143*, 21541–21548.
- (37) Sun, M.; Wu, Z.; Zhang, J.; Chen, M.; Lu, Y.; Yang, C.; Song, Y. Spherical neutralizing aptamer suppresses SARS-CoV-2 Omicron escape. *Nano Today* **2022**, *44*, 101499.
- (38) Chauhan, N.; Xiong, Y.; Ren, S.; Dwivedy, A.; Magazine, N.; Zhou, L.; Jin, X.; Zhang, T.; Cunningham, B. T.; Yao, S.; Huang, W.; Wang, X. Net-shaped DNA nanostructures designed for rapid/sensitive detection and potential inhibition of the SARS-CoV-2 virus. *J. Am. Chem. Soc.* **2022**, DOI: 10.1021/jacs.2c04835.
- (39) Osterman, A.; Iglhaut, M.; Lehner, A.; Späth, P.; Stern, M.; Autenrieth, H.; Muenchhoff, M.; Graf, A.; Krebs, S.; Blum, H.; Baiker, A.; Grzimek-Koschewa, N.; Protzer, U.; Kaderali, L.; Baldauf, H. M.; Keppler, O. T. Comparison of four commercial, automated antigen tests to detect SARS-CoV-2 variants of concern. *Med. Microbiol. Immunol.* **2021**, *210*, 263–275.
- (40) Bekliz, M.; Perez-Rodriguez, F.; Puhach, O.; Adea, K.; Melancia, S. M.; Baggio, S.; Corvaglia, A.-R.; Jacqueroz-Bausch, F.; Alvarez, C.; Essaidi-Laziosi, M.; Escadafal, C.; Kaiser, L.; Eckerle, I. Sensitivity of SARS-CoV-2 antigen-detecting rapid tests for Omicron variant. *Microbiol. Spectrum* **2022**, *10*, e00853-22.
- (41) Xia, X.; Zhang, J.; Lu, N.; Kim, M. J.; Ghale, K.; Xu, Y.; McKenzie, E.; Liu, J.; Ye, H. Pd-Ir core-shell nanocubes: a type of highly efficient and versatile peroxidase mimic. *ACS Nano* **2015**, *9*, 9994–10004.
- (42) Li, J.; Li, Y. Facile synthesis of Pd-Ir nanocubes for biosensing. *Front. Chem.* **2021**, *9*, 775220.
- (43) Li, J.; Li, Y. One-pot high-yield synthesis of Pd nanocubes for Pd-Ir nanocube-based immunoassay of nucleocapsid protein from SARS-CoV-2. *Anal. Bioanal. Chem.* **2021**, *413*, 4635–4644.
- (44) Weber, P. C.; Ohlendorf, D. H.; Wendoloski, J.; Salemme, F. Structural origins of high-affinity biotin binding to streptavidin. *Science* **1989**, *243*, 85–88.
- (45) Wu, N. C.; Wilson, I. A. Structural biology of influenza hemagglutinin: An amaranthine adventure. *Viruses* **2020**, *12*, 1053.
- (46) Spear, P. G.; Longnecker, R. Herpesvirus entry: an update. *J. Virol.* **2003**, *77*, 10179–10185.
- (47) Fletcher, A. J.; Vaysburd, M.; Maslen, S.; Zeng, J.; Skehel, J. M.; Towers, G. J.; James, L. C. Trivalent RING assembly on retroviral capsids activates TRIMS ubiquitination and innate immune signaling. *Cell Host Microbe* **2018**, *24*, 761–775.e6.